Tightly Coupled Bluetooth Enhanced GNSS/PDR System for Pedestrian Navigation in Dense Urban Environments

Jingxian Wang, Xiaolong Mi, Wu Chen, Huan Luo, Ahmed Mansour, Yaxin Li, Yue Yu, and Duojie Weng, *Member, IEEE*

***Abstract*— The performance of the global navigation satellite systems (GNSSs) can be degraded significantly in urban areas and semi-outdoor environments due to the blockage and reflection of GNSS signals. To enhance smartphone positioning in these areas, the integration of pedestrian dead reckoning (PDR) and Bluetooth low energy (BLE) sensors has been proposed and widely developed. However, the current loosely coupled (LC) integration algorithm often fails to achieve accurate positioning in complex urban environments. Challenges such as reliable assessment of GNSS quality, accurate estimation of pedestrian walking direction, and error due to variability of BLE signal (BLES) strength across smartphones and accumulated by PDR remain to be addressed. To achieve precise and continuous location service in urban areas, we have explored the characteristics of BLESs and integrated BLE with GNSS and PDR, enhancing positioning performance through three key algorithms. First, GNSS quality is monitored with the aid of BLESs and PDR results adaptively to minimize their impact on the integration results. Subsequently, the smartphone's orientation and the heading precisely estimated from BLESs are jointly utilized to determine the pedestrian's walking direction. Finally, a tightly coupled (TC) Kalman filter, incorporating distance measurements from strong-signal BLE transmitters, is employed to tackle the device heterogeneity inherent in smartphone BLE sensors and to reduce the cumulative errors associated with PDR positioning. Extensive experiments on different smartphones demonstrate that the proposed system consistently achieves positioning accuracy within 4 m in both urban and semi-outdoor environments.**

***Index Terms*— Bluetooth low energy (BLE), pedestrian positioning, semi-outdoor, smartphone.**

Received 21 June 2024; revised 14 August 2024; accepted 19 August 2024. Date of publication 16 October 2024; date of current version 4 November 2024. This work was supported in part by the General Research Fund of the Research Grants Council of Hong Kong under Grant 15230823; in part by the Smart Cities Research Institute, The Hong Kong Polytechnic University; and in part by the Open Fund of the Key Laboratory of Urban Land Resources Monitoring and Simulation, Ministry of Natural Resources (MNR), under Grant KF-2021-06-125. The Associate Editor coordinating the review process was Dr. Alice Buffi. *(Corresponding author: Duojie Weng.)*

Jingxian Wang, Xiaolong Mi, Wu Chen, Huan Luo, Ahmed Mansour, Yaxin Li, and Yue Yu are with the Department of Land Surveying and Geo-Informatics, The Hong Kong Polytechnic University, Hong Kong, China (e-mail: jingxian.wang@connect.polyu.hk; xiaolong.mi@polyu.edu.hk; wu.chen@polyu.edu.hk; hilary.luo@connect.polyu.hk; ahmed.m.mostafa@connect.polyu.hk; yaxin.pu.li@connect.polyu.hk; michael-yue.yu@polyu.edu.hk).

Duojie Weng was with the Department of Land Surveying and Geo-Informatics, The Hong Kong Polytechnic University, Hong Kong. He is now with the Ministry of Natural Resources (MNR) Key Laboratory for Geo-Environmental Monitoring of Great Bay Area & Guangdong Key Laboratory of Urban Informatics, Shenzhen University, Shenzhen 518060, China (e-mail: wengduojie.lsgi@polyu.edu.hk).

Digital Object Identifier 10.1109/TIM.2024.3481547

I. Introduction

THE increasing demand for location-based services (LBSs) in smartphones has made the global navigation satellite system (GNSS) module the most widely used positioning sensor in these devices. Despite offering global coverage, the GNSS module's accuracy in open areas typically ranges from 3 to 10 m, influenced by factors such as satellite orbit and clock errors, as well as propagation and multipath effects [1]. Errors stemming from satellites and signal propagation can be effectively reduced by employing differential GNSS (DGNSS) technology [2], thereby potentially enhancing positioning accuracy in open areas to within 2 m.

Nevertheless, even with DGNSS technology, the inaccuracies resulting from multipath effects remain unresolved, especially in urban areas and semi-outdoor environments. In such environments, the presence of buildings and other structures exacerbates multipath issues, potentially diminishing the precision of smartphone positioning to an extent of tens of meters [3]. In addition, the prevalence of high-rise buildings in urban areas often results in nonline-of-sight (NLOS) reception of satellite signals [4], further impacting the integrity of satellite-based positioning results.

To address these challenges, the integration of pedestrian dead reckoning (PDR) combined with GNSS, utilizing the smartphone-embedded inertial measurement unit (IMU) [5], has been commonly employed. This integration leverages the IMU's capability for accurate short-term positioning. However, PDR errors accumulate over time. Potential misalignment between the handheld smartphone's orientation and the actual walking direction can further impact the accuracy of PDR calculations [6]. In addition, since PDR calculates relative positions, it is not effective in reducing the absolute positional errors that stem from GNSS.

Fortunately, with the continuous advancement of Internet of Things (IoT) technology, an increasing number of wireless sensors are being installed in cities, such as WiFi [7], Bluetooth low energy (BLE) [8], and ultrawideband (UWB) [9]. These sensors can be used to assist GNSS and PDR to improve positioning performance in complex urban environments. While WiFi devices are typically confined to indoor installations, and UWB support is not widely available in smartphones, BLE stands out as a more versatile option. BLE's adaptability to a variety of scenarios, its scalability, and the prevalent integration of Bluetooth transceivers in

contemporary smart devices combine to render BLE a highly effective and feasible choice for augmenting urban navigation systems [10].

Numerous studies have explored the integration of GNSS, PDR, and BLE [11], [12]. However, the accuracy of GNSS in dense urban environments remains challenging to estimate, potentially leading to significant errors that can negatively impact the performance of integrated positioning systems [13]. In addition, due to installation constraints and cost considerations, BLE transmitters in these environments are typically sparsely installed, resulting in fewer and weaker BLE signals (BLESs) compared to indoor scenarios, which tends to yield less than optimal positioning outcomes from BLE. Consequently, loosely coupled (LC) integrations, commonly used in these studies, are less effective in outdoor environments [14].

In contrast, tightly coupled (TC) integration with BLE is more suitable as it enables a more comprehensive utilization of BLE data, thereby enhancing the overall positioning accuracy [15], [16]. Nevertheless, a significant challenge remains in the form of device heterogeneity among different smartphone-embedded Bluetooth sensors, which leads to variations in BLES strength at the same location across different devices [17]. Such discrepancies can impair the precision of position corrections achieved through proximity to BLE transmitters and the estimated distances based on BLESs, potentially resulting in reduced positioning performance for certain devices.

Therefore, to ensure precise pedestrian positioning in dense urban environments, three crucial challenges must be addressed. First, current methods cannot estimate GNSS errors (GEs) with both precision and adaptability, leading to inaccurate error propagation in integrated positioning systems, thereby affecting their performance. Second, misalignment between the smartphone's orientation and the pedestrian's walking direction introduces errors in PDR calculations. Finally, variations in Bluetooth chipsets and antenna designs across smartphones lead to biases in BLE received signal strength indicator (RSSI) values. Without accurately estimating these biases, distance calculations based on RSSI are biased, and the accuracy of proximity algorithms is affected by preset RSSI thresholds, ultimately impacting the performance of BLE-based positioning algorithms and the integrated system.

To effectively resolve these issues, it is essential to harmonize the proximity positioning method of BLE with its distance estimation capabilities within the GNSS/PDR integration system. Thus, we proposed a TC BLE-enhanced GNSS/PDR system. The key contributions of this study are summarized as follows.

1) We achieved accurate adaptive GE estimation by leveraging data from BLE locations and PDR outcomes. This significantly reduces the impact of imprecise GE assessments on position integrations in dense urban environments.
2) The pedestrian's walking direction is determined by jointly using the smartphone's orientation and heading data estimated from BLESs, effectively minimizing PDR positional errors caused by misalignment between the smartphone's orientation and the pedestrian's actual direction, enhancing PDR positioning accuracy.
3) Our TC approach evaluates the RSSI bias (RB) in the smartphone-embedded BLE sensor, reducing the impact of using different smartphone models on the accuracy of BLE-based positioning algorithms. In addition, distances estimated from strong-signal BLE transmitters are integrated into the TC system to diminish cumulative errors in PDR positioning, achieving long-term accurate positioning even with sparsely installed BLE transmitters.

The organization of this article is as follows. Section II reviews related works. Section III details the algorithms of the enhanced system. Section IV presents the experimental results evaluating the precision and robustness of the proposed system. Section V concludes this article.

II. Related Works

In this section, a comprehensive review of previous literature on BLE, IMU, and multisensor integrated positioning algorithms is presented, and the challenges faced by each approach are discussed.

A. BLE-Based Positioning Algorithm

There exists a wide array of BLE-based positioning algorithms, but due to the fact that many handheld terminals do not support newer methods like angle of arrival (AOA) and angle of departure (AOD), the positioning solutions typically employed in widespread environments can be categorized into three main types: the BLE proximity detection approach, the trilateration approach, and the fingerprinting approach.

Proximity implies that when the mobile device detects a BLE device, the mobile device is deemed to be at the same location as the BLE device [18]. This approach is straightforward to implement. However, it is evident that a clear limitation is that the localization accuracy is deeply dependent on beacon density. Several strategies have been proposed to enhance its performance. Yin et al. [19] fine-tuned a metric function to determine the optimal RSSI threshold. This threshold strikes a balance between producing abundant low-detail reports and a limited number of highly insightful ones, consequently enhancing the performance of proximity-based positioning algorithms. Chawathe [20] employed a map, which encompasses the position and identifier details of BLE devices, to expedite BLE device detection, subsequently enhancing the accuracy of proximity positioning.

Trilateration determines the position of the rover station by measuring the distance to at least four known base stations [21]. The accuracy of distance measurement directly impacts the positioning performance. Generally, there are two types of distance estimation methods. One is based on RSSI and a signal propagation model to estimate the distance between the user and the base station. The effectiveness of this approach is closely related to the selection of the model and the estimation of its parameters [10]. The other method relies on the time of flight (ToF) of the signal. However, due to Bluetooth signals being narrowband, ToF faces limited resolution of the available clocks to measure time intervals [22].

Fingerprinting captures a distribution map of spatially variable parameters in the database during its offline phase. In the online phase, these parameters are measured and matched with the existing database to obtain the location of users [23]. Traditionally, constructing and maintaining the database requires significant time and manpower resources. However, the autonomous creation of these databases, facilitated by methods like crowdsourcing [8], can be used to generate self-updated databases.

The accuracy of these BLE solutions can be compromised due to device heterogeneity issues. In other words, the RSSI values vary across different devices at an identical location, stemming from variations in antenna types, radio frequency circuit designs, and other factors. Fortunately, there is a discernible pattern in device heterogeneity. Typically, the RSSI error induced by device heterogeneity is perceived as a constant bias. Thus, techniques such as signal strength differentiation [24] or machine learning approaches [17] can be employed to mitigate the effects of hardware variations.

B. IMU-Based Positioning Algorithm

IMU-based positioning algorithms can be divided into two main categories: inertial navigation system (INS) and PDR. INS provides positions, velocities, and attitudes with the integration of acceleration and angular velocity [25]. However, due to the poor performance of the built-in IMU in smartphones, the INS results diverge quickly [25]. To mitigate the accumulating and drifting errors in INS, several techniques have been adopted. For example, Tao et al. [26] utilize adaptive zero-velocity update (ZUPT) as well as heuristic drift reduction (HDR) to enhance the availability and integrity of the foot-mounted IMU-based positioning method. Due to the inherent difficulty in accurately detecting the zero-velocity state when utilizing handheld devices, the performance of ZUPT and HDR is considerably diminished.

To mitigate the potential impact of erroneous utilization of constraints like ZUPT, PDR has become more popular in pedestrian positioning [27]. It mainly consists of three key components: step detection, step length estimation, and heading calculation (HC). Step detection plays a critical role in pedestrian localization, as it serves as a fundamental requirement for dead reckoning (DR) algorithms. Various techniques such as peak detection [28], zero-crossing [29], fast Fourier transform (FFT) [30], and wavelet transform [31] are utilized to ensure precise identification of individual steps. The step length is influenced by various factors including step frequency, acceleration magnitude within each step, walking speed, and user height [32]. Several reliable estimation algorithms have been developed for determining step length, such as constant models [33], linear models [34], nonlinear models [35], and artificial intelligence (AI) models [36]. Heading information can be simply and conveniently obtained from the magnetometer [37]. However, in urban environments with a higher presence of ferromagnetic materials, the magnetic field environment becomes more variable. As a result, the direction obtained from the magnetometer often tends to be inaccurate. Moreover, it is crucial to address the misalignment between the direction of the handheld smartphone and the actual walking directions. In order to address this issue, several methods, including principal component analysis (PCA) [38], forward and lateral acceleration modeling (FLAM) [6], and frequency analysis of inertial signals (FIS) [39], have been proposed. However, due to the limited precision of the low-cost IMU embedded in smartphones, these methods only perform well under specific hand movement features [40]. Therefore, it is generally more effective to integrate PDR with other positioning methods.

C. Multisensor Integrated Positioning Algorithm

Each sensor has its unique strengths and weaknesses. By merging various sensors, their advantages can complement each other. Integrated navigation systems are mostly nonlinear, so nonlinear filtering methods are generally employed, such as the particle filter (PF), extended Kalman filter (EKF), and unscented Kalman filter (UKF). PF stands out in nonlinear or non-Gaussian systems [41]. However, its efficacy hinges on the particle count, implying that greater computational intensity is required for optimal estimation. Comparing EKF to UKF, UKF has a higher computational cost than EKF, while the precision gain in integrated navigation is insignificant [42]. Thus, for real-time integrated navigation systems, EKF is more practical.

Integration strategy can be categorized into LC scheme and TC scheme. LC scheme is more common, where the positioning results obtained from BLE-based methods are used to correct those from IMU-based methods [16]. This approach is suitable when BLE devices are densely deployed. If the installation of BLE devices is sparse, the performance of the integration may be affected. In the case of the TC scheme, even with fewer BLE devices, the distance information provided by BLE can constrain the IMU-based positioning results, enhancing the usability of BLE devices [43]. Since many smartphones still don't support raw measurement outputs for GNSS, this article will not delve further into the GNSS TC scheme.

GNSS positioning performance can be severely degraded to more than 80 m by satellite signal blockage and severe multipath effects [44]. In the GNSS LC scheme, the precision of the integrated results can be negatively influenced by imprecise GNSS results if the GE estimation is erroneous. Attaining high accuracy in GE estimation independently presents a significant challenge. To address this, additional information sources are utilized for more accurate GE estimation.

III. Enhanced Integrated System

In urban canyons, the GNSS performance is severely degraded, while PDR can only offer relative location results. Hence, there is an urgent need to develop a novel system to estimate positions precisely. To support the development of smart cities, smart lampposts have been widely installed all over the world. As illustrated in Fig. 1, we have designed these lampposts to be equipped with BLE transmitters operating at two different transmission powers (TPs): weak-signal and strong-signal BLE transmitters, aimed at providing accurate positioning services to citizens in urban areas by combining signals from BLE transmitters with different TP. The weak-signal BLE transmitters are designed for proximity positioning and direction provision. With a TP of −20 dBm,

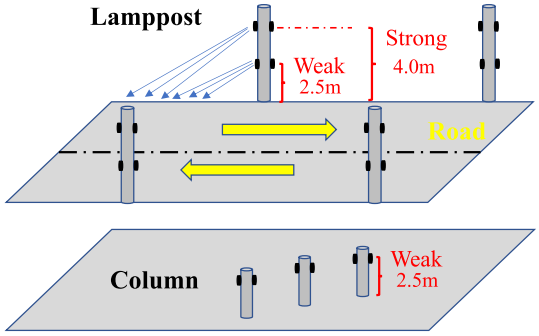

Fig. 1. BLE transmitter installation schematic.

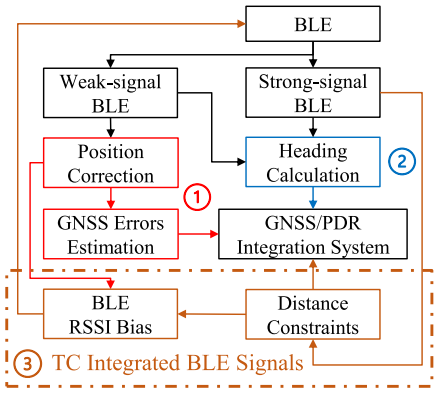

Fig. 2. Overview of the TC BLE-enhanced GNSS/PDR integration system.

these transmitters allow pedestrians to receive signals within a 5-m radius of the lamppost. Due to the internal materials of the lamppost blocking the Bluetooth signal, each lamppost has one transmitter installed in the front and one in the back at a height of 2.5 m, along the direction of the road. Similarly, the strong-signal BLE transmitters are installed at a height of 4 m on each lamppost. These transmitters are designed for distance measurement and direction indication tasks, with a TP of 4 dBm, enabling pedestrians to receive signals within a 100-m radius of the lamppost. In addition, similar setups with weak-signal BLE transmitters are also installed on pillars in semi-outdoor areas.

The major and minor values of BLE transmitters, along with their positional information and directional relationships, are stored in the representational state transfer (REST) application programming interface (API) server in a JavaScript Object Notation (JSON) array format. This information can be obtained using a hypertext transfer protocol secure (HTTPS) "GET" method with the specified API uniform resource locator (URL). This step is performed during system initialization and testing has shown that it takes approximately 700 ms.

This article proposes the GNSS/PDR integration system by integrating TC BLE, as illustrated in Fig. 2. The diagram delineates the core components in black, with the red, blue, and brown colors indicating the optimization techniques newly introduced in this research. First, the integration system employs weak-signal BLE for positional corrections and adaptive GNSS quality assessments to refine the positioning results and reduce the negative impact of suboptimal GNSS data on the integration outcome. Second, it computes the pedestrian's walking direction by synthesizing heading information from both strong-signal and weak-signal BLE with the smartphone's orientation. This information is crucial for PDR calculations, significantly curtailing positional errors caused by any misalignment between the smartphone's orientation and the pedestrian's actual direction. Third, upon the detection of strong-signal BLE, the system utilizes the distances between the user and BLE transmitters as constraints within the integrated system, significantly reducing the accumulation of PDR positioning errors over time. Simultaneously, when position corrections from weak-signal BLE are received, the RB of the BLE sensor is estimated, effectively addressing the device heterogeneity prevalent in smartphone BLE sensors.

The EKF is used to integrate GNSS/PDR/BLE. Traditionally, the state equation of the EKF is

$$\boldsymbol{X}_i = \boldsymbol{F}\boldsymbol{X}_{i-1} + \boldsymbol{G}\boldsymbol{W}_{i-1} \tag{1}$$

where the subscript i indicates the time instance, $\boldsymbol{X}_{i-1}$ denotes the state vector at epoch $i-1$, $\boldsymbol{F}$ denotes the transition matrix, $\boldsymbol{G}$ denotes the system noise matrix, and $\boldsymbol{W}_{i-1}$ denotes the system noise vector with the covariance matrix $\boldsymbol{Q}$: $\boldsymbol{W}_{i-1} \sim N(0, \boldsymbol{Q}_{i-1})$.

The state vector used in this system is shown below

$$\boldsymbol{X} = [\delta N \quad \delta E \quad \delta S \quad \delta\theta]^{\mathrm{T}} \tag{2}$$

where δN and δE represent the error of the northing and easting coordinates of the pedestrian, respectively. The δS serves as the error of the scale factor of step length. $\delta\theta$ is the heading error of the pedestrian. Since they are all related to PDR, we conducted a series of walking experiments under a dynamic capture system while holding the smartphone. Using the millimeter-level precision of the dynamic capture system as a benchmark, we compared it with the measured PDR results. After statistical analysis, we obtained the parameters for the Q matrix.

The measurement equation is

$$\boldsymbol{Z}_i = \boldsymbol{H}_i\boldsymbol{X}_i + \boldsymbol{V}_i \tag{3}$$

where $\boldsymbol{Z}_i$ represents the measurement vector, $\boldsymbol{H}_i$ denotes the measurement matrix, and $\boldsymbol{V}_i$ stands for the measurement noise with covariance matrix $\boldsymbol{R}$: $\boldsymbol{V}_i \sim N(0, \boldsymbol{R}_i)$.

Generally, the measurement vector provided by GNSS is

$$Z_{\mathrm{GNSS}} = \begin{bmatrix} N_{\mathrm{GNSS}} - N_{\mathrm{PDR}} \\ E_{\mathrm{GNSS}} - E_{\mathrm{PDR}} \end{bmatrix} \tag{4}$$

where N and S denote the northing and easting coordinates, the subscript GNSS indicates that this value is obtained from GNSS, and the subscript PDR indicates that this value is obtained from PDR.

Since the lampposts are sparsely installed, typically 30–40 m apart, the signal fluctuations of strong-signal BLE transmitters are significant. Combined with the presence of RB, directly using RSSI to calculate distance for trilateration results in unreliable outcomes. The proximity method, which requires only one beacon for positioning, is suitable for scenarios with sparse beacon deployment. According to the proximity principle, the mobile device is deemed to be at the same location as the BLE device. In this study, the weak-signal BLE transmitters have a TP set to -20 dBm, allowing users

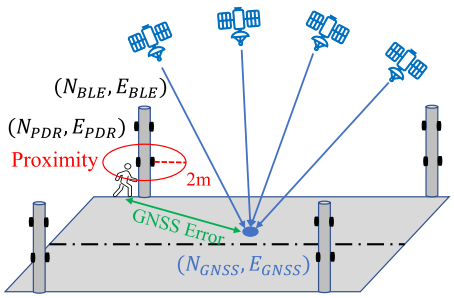

Fig. 3. GEs estimation.

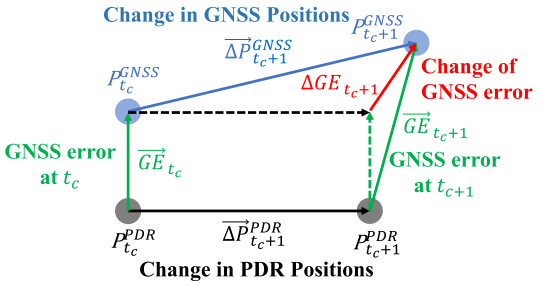

Fig. 4. Estimation of GEs with the aid of BLE and PDR.

to receive their signals within a 5-m radius of the lamppost. Experiments on the detection method, detailed in our previous study [12], indicate that the positional error after correction is less than 2 m. Hence, when approaching weak-signal BLE transmitters, the measurement vector provided by BLE is

$$Z_{\text{BLE}} = \begin{bmatrix} N_{\text{BLE}} - N_{\text{PDR}} \\ E_{\text{BLE}} - E_{\text{PDR}} \end{bmatrix} \tag{5}$$

where the subscript BLE indicates that this value is obtained from the coordinates of these BLE transmitters. The corresponding R matrix parameters were set by statistically analyzing the errors between the detected positions and the actual positions of the weak-signal BLE transmitters through multiple tests of the proximity method.

In the following parts, Section III-A assesses the quality of GNSS data adaptively to dynamically adjust the precision of GNSS data in the integration. Section III-B calculates the pedestrian's walking direction to improve the PDR performance. Section III-C estimates the RB of the BLE sensor and uses distance measurements from BLESs to enhance PDR accuracy.

A. Adaptive Assessment of GNSS Quality

Currently, many GNSS/PDR integrated systems utilize GNSS-provided error estimates as the variance for the measurement vector provided by GNSS [5], [45]. However, the variability of GE, affected by numerous factors such as ionospheric conditions and local environment, complicates the accurate assessment of GNSS data quality without supplementary instruments [46]. Hence, this can result in an underestimation of the actual errors. Therefore, the precision of GNSS/PDR integrations can be compromised by these imprecise GE estimations.

To achieve precise and adaptive estimation of GEs, this study introduces positional data from BLE transmitters for GE estimation. As illustrated in Fig. 3, when users are in proximity to weak-signal BLE transmitters, their positions are corrected according to (5). At this moment, the user's position is considered accurate. Consequently, the distance between the GNSS-derived position and this corrected user position represents the GE

$$\overrightarrow{\text{GE}}_{t_c} = \begin{bmatrix} \text{GE}_N \\ \text{GE}_E \end{bmatrix} = \begin{bmatrix} N_{\text{GNSS}} - N_{\text{PDR}} \\ E_{\text{GNSS}} - E_{\text{PDR}} \end{bmatrix} \tag{6}$$

where $\overrightarrow{\text{GE}}_{t_c}$ is the GE at the position corrected time t_c, GE_N is the GE in the north direction, and GE_E is the GE in the east direction.

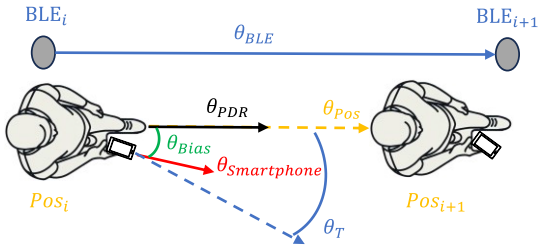

Fig. 5. Illustration of the relationship between pedestrian walking direction θ_{PDR} smartphone's orientation $\theta_{\text{Smartphone}}$ and BLE-derived heading θ_{BLE}.

Since the installation spacing of weak-signal BLE transmitters typically ranges between 30 and 50 m and the fact that GE is inherently dynamic, it becomes essential to continuously estimate the GE in real time. As the PDR's results are considered accurate over short durations, the difference between GNSS positional changes and PDR positional changes can be interpreted as variations in GEs. This relationship is depicted in Fig. 4. Consequently, the GE at the time t_i can be determined using the following equation:

$$\overrightarrow{\text{GE}}_{t_i} = \overrightarrow{\text{GE}}_{t_c} + \sum_{t=t_c+1}^{t_i} \left(\overrightarrow{\Delta P}_t^{\text{GNSS}} - \overrightarrow{\Delta P}_t^{\text{PDR}} \right) \tag{7}$$

where $\overrightarrow{\Delta P}_t^{\text{GNSS}}$ is the position change of GNSS, and $\overrightarrow{\Delta P}_t^{\text{PDR}}$ is the position change of PDR. Based on (7), the relatively accurate GE for each epoch is determined. This error can then serve as the covariances for the measurement vector supplied by the GNSS R_{GNSS} in the EKF

$$R_{\text{GNSS}} = \begin{bmatrix} \overrightarrow{\text{GE}}_N^2 & 0 \\ 0 & \overrightarrow{\text{GE}}_E^2 \end{bmatrix}. \tag{8}$$

B. Pedestrian Walking Direction Calculation for PDR

In PDR calculations, existing methods typically assume that the smartphone's heading is equivalent to the pedestrian's walking direction [8]. Nonetheless, as depicted in Fig. 5, the direct use of the smartphone's orientation in PDR calculations can cause inaccuracies in positioning, since the real walking direction of pedestrians might not match the orientation of their smartphones. This discrepancy often arises because pedestrians' hands may swing as they walk, causing a misalignment between the device's orientation and their actual path of movement. Therefore, it is essential to differentiate between the pedestrian's walking direction and the smartphone's heading to ensure more accurate positioning. Some

approaches consider the misalignment between the handheld smartphone's direction and the actual walking directions, while the limited precision of the low-cost IMU embedded in smartphones means that these methods are only effective with particular hand movement characteristics [40]. If a pedestrian were to consistently walk in the heading indicated by BLE, then using the BLE heading as the pedestrian's heading would significantly mitigate the issues. However, real-life pedestrian movements are not so linear; people might sidestep or alter their paths due to obstacles, to avoid others, or for various other reasons. Thus, it is not feasible to directly use the BLE heading for PDR position calculation.

Since the detailed calculation algorithms of $\theta_{\text{Smartphone}}$ and θ_{BLE} have been illustrated in our previous study [12], they will not be revisited in this article. This article aims to combine the smartphone's orientation based on IMU $\theta_{\text{Smartphone}}$ with the BLE-derived headings θ_{BLE} to provide an accurate estimate of the pedestrian walking direction θ_{PDR} for PDR calculation. The proposed method is outlined in (9). The first step involves evaluating the pedestrian's movement pattern to determine whether it is linear or involves turns at corners. If the integral of the difference between θ_{BLE} and $\theta_{\text{Smartphone}}$ remains below our predefined threshold θ_T, over a certain period (3 s, as applied in our study), it indicates that the pedestrians are moving straight without any turns, and thus, θ_{PDR} is constrained to the BLE heading. Conversely, if the threshold is exceeded, the method defaults to using $\theta_{\text{Smartphone}}$. This strategy effectively reduces positioning errors stemming from discrepancies between the smartphone's orientation $\theta_{\text{Smartphone}}$ and the actual walking direction θ_{PDR}, particularly during hand swing, while still accommodating the precision required for abrupt directional changes

$$\theta_{\text{PDR}} = \begin{cases} \theta_{\text{BLE}}, & \int_i^{i+n} (\theta_{\text{BLE}} - \theta_{\text{Smartphone}})dt < \theta_T \\ \theta_{\text{Smartphone}}, & \text{Others.} \end{cases} \tag{9}$$

The premise of (9) is that $\theta_{\text{Smartphone}}$ is accurate. However, due to the low quality of the smartphone's built-in IMU, the calculated orientation of the smartphone tends to diverge over time. Hence, when the heading θ_{BLE} is obtained from BLE, it can be used to replace the current orientation of the smartphone $\theta_{\text{Smartphone}}$ to correct the heading. However, a bias θ_{Bias} may exist between the BLE headings and the smartphone's true heading since the smartphone's heading $\theta_{\text{Smartphone}}$ tends to vary due to the dynamics of walking

$$\theta_{\text{Smartphone}} = \theta_{\text{BLE}} + \theta_{\text{Bias}}. \tag{10}$$

Hence, the main heading θ_{Pos}, which was estimated from a line regression of previous positions, is utilized to approximate θ_{Bias}

$$\theta_{\text{Smartphone}} = \theta_{\text{BLE}} + (\theta_{\text{Pos}} - \theta_{\text{Smartphone}}). \tag{11}$$

C. TC Integration With BLESs for Device Heterogeneity Mitigation and Advanced Positioning

There has been extensive research on the LC scheme with BLE [16]. However, this approach is only suitable when BLE devices are densely deployed. Considering factors such as cost, outdoor is difficult to deploy beacons as densely as indoors. If the installation of BLE devices is sparse, the performance of the LC integration may be affected. However, for the TC scheme, even with fewer BLE devices, the distance information provided by BLE can constrain the IMU-based positioning results, enhancing the usability of BLE devices [47]. However, most existing algorithms do not take into account the RB between different smartphones' BLE sensors [43].

It has been illustrated in our previous study [12] that a threshold RSSI_T is used for the detection of proximity to the weak-signal BLE transmitters. Due to the presence of device heterogeneity, the RSSI_T values differ among devices. there exists a bias RSSI_b between the RSSI'_T value of the user's device and RSSI_T of the phone tested during factory calibration

$$\text{RSSI}'_T = \text{RSSI}_T - \text{RSSI}_b. \tag{12}$$

This kind of bias also presents challenges when leveraging the RSSI value from strong-signal BLE to estimate distances. Generally speaking, the correlation between the RSSI value and the distance of propagation, as described by the path loss model, is expressed as

$$\text{RSSI} = \text{RSSI}_0 - 10\eta \log_{10}(d/d_0) \tag{13}$$

where RSSI is the received signal strength indicator at d which is the distance between the BLE sensor and the smartphone, RSSI_0 is the received signal strength at the reference distance d_0 which usually takes 1 m for convenient calculation, and η is the path loss exponent which is an empirical value. Then, the distance d can be estimated as

$$d = 10^{\left(\frac{\text{RSSI}_0 - \text{RSSI}}{10\eta}\right)}. \tag{14}$$

When accounting the bias RSSI_b between the RSSI_0 value of the user's device and RSSI_C of the phone tested during factory calibration, it is possible to derive the following equation:

$$\text{RSSI}_0 = \text{RSSI}_C - \text{RSSI}_b. \tag{15}$$

Thus, (14) and (15) can be combined as follows:

$$d = 10^{\left(\frac{\text{RSSI}_C - \text{RSSI}_b - \text{RSSI}}{10\eta}\right)} = \hat{d} \cdot 10^{\left(\frac{-\text{RSSI}_b}{10\eta}\right)}. \tag{16}$$

According to (16), we can obtain

$$\hat{d} = d \cdot 10^{\left(\frac{\text{RSSI}_b}{10\eta}\right)}. \tag{17}$$

To linearize (17), using the Taylor expansion at the point $\text{RSSI}_b = 0$ can get the following:

$$\hat{d} = d + \frac{d \cdot \ln 10}{10\eta} \cdot \text{RSSI}_b. \tag{18}$$

RSSI_b can be modeled as a random walk process

$$\dot{\text{RSSI}}_b = \omega_{\text{RSSI}_b} \tag{19}$$

where ω_{RSSI_b} is white noise.

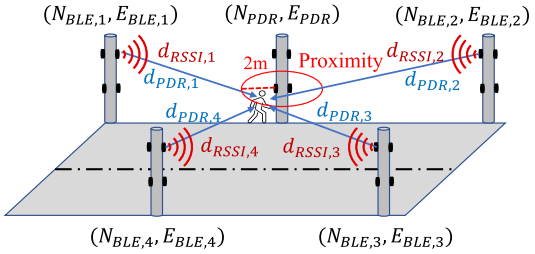

Fig. 6. BLE RB estimation with TC EKF.

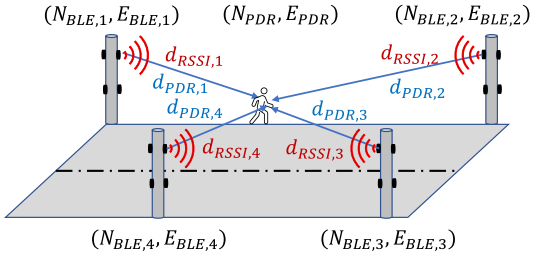

Fig. 7. TC integration with BLESs.

1) BLE RB Estimation in TC Integration: It is evident in our previous study [12] that the proximity to the weak-signal BLE transmitters can provide 2-m accuracy positions. As illustrated in Fig. 6, when users approach these weak-signal BLE transmitters, their positions can be corrected using (5). Subsequently, user devices detect RSSI from strong-signal BLE transmitters mounted on other lampposts, which can be utilized to compute d_{RSSI} through (16). As the coordinates of these BLE transmitters can be obtained from the server, the distance d_{PDR} between the current position of the user and strong-signal BLE transmitters can be calculated by the following equation:

$$d_{\text{PDR}} = \sqrt{(N_{\text{BLE}} - N_{\text{PDR}})^2 + (E_{\text{BLE}} - E_{\text{PDR}})^2 + (U_{\text{SBLE}} - U_{\text{PDR}})^2} \tag{20}$$

where U_{SBLE} denotes the installation height of the strong-signal BLE transmitters, set at 4 m, and U_{PDR} represents the estimated height of hand-held devices based on the user's height. Thus, RSSI_b can be incorporated as an additional state within the TC EKF. The adjustment to the state vector is illustrated in the following equation:

$$\boldsymbol{X} = [\delta N \quad \delta E \quad \delta S \quad \delta\theta \quad \text{RSSI}_b]^{\text{T}}. \tag{21}$$

The Q matrix parameter for RSSI_b was obtained from statistical analysis of the deviations in RSSI values received by different smartphones at the same location.

These distances (at least one) can be used as additional measurement vectors like

$$Z_{\text{Distance}} = \begin{bmatrix} d_{\text{RSSI},1} - d_{\text{PDR},1} \\ \cdots \\ d_{\text{RSSI},n} - d_{\text{PDR},n} \end{bmatrix}. \tag{22}$$

The corresponding R matrix parameters were set by statistically analyzing the errors between the measured distances from the strong-signal BLE transmitters and the known distances at those locations.

The measurement matrix is given by (23), as shown at the bottom of the next page.

Due to the obstruction caused by the human body, the strength of the Bluetooth signal received by the phone can be influenced. Hence, only the distances corresponding to the strong-signal BLE transmitters located in the direction of pedestrian movement are specifically chosen to be used in (22). As illustrated in Fig. 6, only signals emitted from the second and third lampposts are utilized in the calculations. Using signals from all the strong-signal BLE transmitters could potentially worsen the results because the signal attenuation caused by human body obstruction is challenging to estimate accurately, leading to incorrect weight assignment for these observations.

2) Positioning Performance Enhancement via TC Integration With Strong-Signal BLE: Although we have optimized step detection and step length estimation in our prior research [12], the error in the forward direction of PDR still accumulates significantly over time due to the sparse installation of BLE transmitters, as demonstrated in Fig. 7. Hence, after estimating the BLE RB, when there is no proximity detection from the weak-signal BLE transmitters, the TC scheme leverages distances directly estimated from strong-signal BLE transmitters as observations to seamlessly merge with PDR results, enhancing the accuracy of PDR positioning. This approach optimizes the utilization of available BLE data, ensuring effective integration even in scenarios where signals from fewer than four strong-signal BLE transmitters are available. The additional measurement vectors are defined as follows:

$$Z_{\text{BLETC}} = \begin{bmatrix} d_{\text{RSSI},1} - d_{\text{PDR},1} \\ \cdots \\ d_{\text{RSSI},n} - d_{\text{PDR},n} \end{bmatrix}. \tag{24}$$

Since RSSI_b has already been computed in Section III-B, the measurement matrix for this part is presented as follows:

$$H_{\text{BLETC}} = \begin{bmatrix} \dfrac{N_{\text{BLE}} - N_{\text{PDR},1}}{d_{\text{PDR},1}} & \dfrac{E_{\text{BLE}} - E_{\text{PDR},1}}{d_{\text{PDR},n}} & 0 & 0 & 0 \\ \cdots & \cdots & \cdots & \cdots & \cdots \\ \dfrac{N_{\text{BLE}} - N_{\text{PDR},n}}{d_{\text{PDR},n}} & \dfrac{E_{\text{BLE}} - E_{\text{PDR},1}}{d_{\text{PDR},n}} & 0 & 0 & 0 \end{bmatrix}. \tag{25}$$

IV. Experiments and Results

To assess the efficacy of our proposed algorithms, two distinct smartphones, the Pixel 7 Pro and Mate 20 Pro, were used to conduct three experiments. The performance parameters of the smartphone-embedded sensors are listed in Table I. It can be observed that although different IMU models were used, their performance is similar. For parameters related to the BLE in our integrated system, such as RSSI_T and RSSI_0, they are configured based on the Pixel 7 Pro. Hence, we can assume that the Pixel 7 Pro does not exhibit any RB.

TABLE I
PERFORMANCE PARAMETERS OF SMARTPHONE-EMBEDDED SENSORS

Smartphone	Pixel 7 Pro	Mate 20 Pro
IMU	LSM6DSV	ICM20690
Accelerometer noise ($\mu g/\sqrt{Hz}$)	100	100
Gyroscope noise ($mdps/\sqrt{Hz}$)	± 2.8	± 4
Bluetooth (Supported Version)	WCN3990 (5.2)	Hi1103 (5.0)

However, compared to other smartphones like the Mate 20 Pro, which uses different Bluetooth chips and antenna designs, there may be a bias in the received RSSI values under the same conditions. Therefore, we conducted the first experiment to verify the existence of the RB of the BLE sensor. Then, the second experiment delved into evaluating the performance of our adaptive GE estimation algorithm, the approach for calculating pedestrian walking direction, and the application of BLES constraints in our enhanced GNSS/PDR/BLE TC integration system on a smartphone without BLE RB (Pixel 7 Pro). Finally, the last experiment was dedicated to quantifying the performance of the aforementioned algorithms, along with our proposed RB estimation algorithm, to determine if performance declines when using a smartphone that exhibits RB (Mate 20 Pro).

A. Verification of the Existence of the RB in BLE Sensors

To verify the existence of the RB in BLE sensors, we used two distinct smartphones: the Pixel 7 Pro and Mate 20 Pro. In this test, the BLE transmitter is installed at a height of 1 m, aligning with the height of handheld devices. At distances of 1, 2, and 4 m from the BLE transmitter, these two smartphones were held facing the BLE transmitter to take 200 readings at each distance. The raw data are shown in Fig. 8. Applying a Gaussian fit to the acquired data enabled us to determine the mean RSSI values.

Table II offers a comparative insight into these results. Notably, across all measured distances, the Mate 20 Pro registers a consistently lower RSSI value than the Pixel 7 Pro. The disparities are evident: 3.48 dBm at 1 m, 2.99 dBm at 2 m, and 2.91 dBm at 4 m. These findings underscore the inherent variability between BLE sensors in different smartphones. Despite being under analogous conditions, the reception capabilities and sensitivity can differ markedly. Since parameters related to the BLE, such as RSSI_T and RSSI_0, are configured based on the Pixel 7 Pro, we assume that the Pixel 7 Pro does not exhibit any RB. Considering that RSSI values are typically presented as integers, according to (14), RSSI_b for the Mate 20 Pro would be 3 dBm.

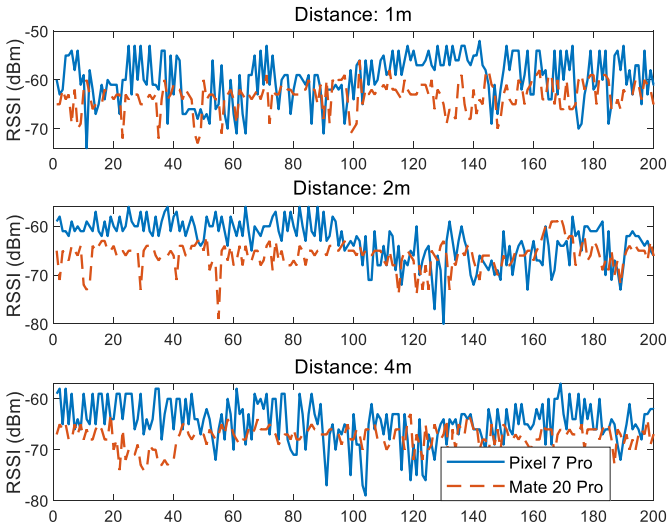

Fig. 8. RSSI measurements of BLE sensors at various distances.

TABLE II
RSSI MEASUREMENTS ACROSS DIFFERENT SMARTPHONES AT VARYING DISTANCES

Distance	**1 m**	**2 m**	**4 m**
Pixel 7 Pro	-59.77 dBm	-62.85 dBm	-64.57 dBm
Mate 20 Pro	-63.25 dBm	-65.84 dBm	-67.48 dBm
Difference	3.48 dBm	2.99 dBm	2.91 dBm

B. Evaluation of Positioning Performance Enhancement of the Proposed Algorithms on a Smartphone Without BLE RB

To assess the performance of the adaptive GE estimation algorithm, the approach for determining pedestrian walking direction, and the application of BLES constraints in our enhanced GNSS/PDR/BLE TC integration system, we implemented it on the Pixel 7 Pro, a smartphone without BLE RB, and conducted an experiment in a typical mixed urban and semi-outdoor environment. The experimental route is depicted in Fig. 9. This route represents a typical urban scenario where a pedestrian moves from one building to another. The route starts from the top right of the map and proceeds through a semi-outdoor pathway covered by a glass canopy. It then follows the sidewalk adjacent to the building before concluding at the building's main entrance. The total distance is approximately 380 m. As shown in Fig. 10, we pass by five lampposts and seven columns along this route, which are equipped with 24 weak-signal BLE transmitters and ten strong-signal BLE transmitters. The BLE transmitters used in our test are custom "Road Studs" models from April Brother Technology Company Ltd. [48]. These transmitters have a

$$H_{\text{Distance}} = \begin{bmatrix} \frac{N_{\text{BLE}} - N_{\text{PDR},1}}{d_{\text{PDR},1}} & \frac{E_{\text{BLE}} - E_{\text{PDR},1}}{d_{\text{PDR},n}} & 0 & 0 & -\frac{d_{\text{PDR},1} \cdot \ln 10}{10\eta} \\ \cdots & \cdots & \cdots & \cdots & \cdots \\ \frac{N_{\text{BLE}} - N_{\text{PDR},n}}{d_{\text{PDR},n}} & \frac{E_{\text{BLE}} - E_{\text{PDR},1}}{d_{\text{PDR},n}} & 0 & 0 & -\frac{d_{\text{PDR},n} \cdot \ln 10}{10\eta} \end{bmatrix} \tag{23}$$

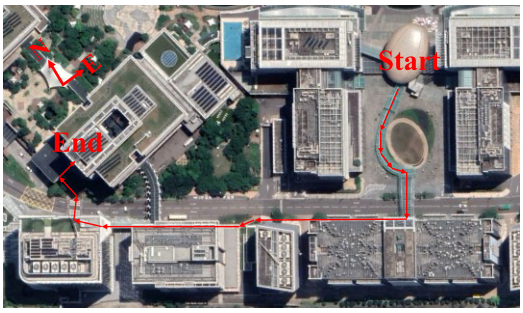

Fig. 9. Experimental route.

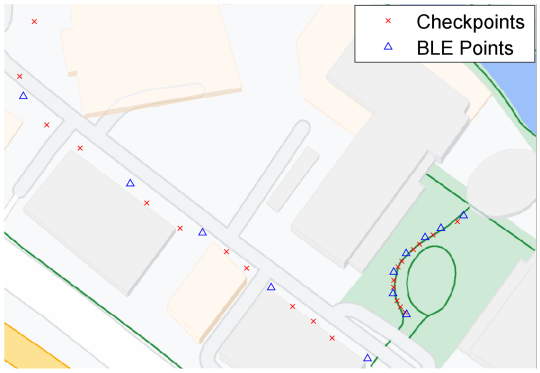

Fig. 10. BLE devices installed points and checkpoints.

protection level of IP67, making them suitable for outdoor use and contain omnidirectional PCB antennas to ensure that a wider range of users can receive the signal.

To accurately measure the positioning accuracy of the integrated system, we selected 22 easily identifiable checkpoints evenly distributed between locations where BLE transmitters are installed. We precisely measured their positions using a total station. During testing, our program recorded the necessary sensor data in sequence. When reaching a checkpoint, we manually entered the checkpoint's number, and the program recorded the number, time, and both GNSS and system-calculated positions. After the experiment, we exported these position data to compare with the true positions we measured, quantitatively evaluating the positioning accuracy.

In this experiment, considering the practical requirement for the battery life of BLE transmitters, the broadcasting frequency of the BLE transmitters is set to 2.5 Hz to control power consumption, while the IMU sampling frequency is set to 50 Hz. Four GNSS/PDR/BLE integration configurations are chosen for performance comparison. The computational complexity of these configurations is also listed below in the form of $O(n^2 + k^{2.4})$, where n is the dimension of the state vector, and k is the dimension of the measurement vector.

1) *LC:* Basic LC GNSS/PDR/BLE integration from our prior study, $O(4^2 + 4^{2.4})$.
2) *LC + GE:* LC with GE estimation, $O(4^2 + 4^{2.4})$.
3) *LC + GE + HC:* LC with GE estimation and HC, $O(4^2 + 4^{2.4})$.
4) *TC + GE + HC + BLES:* Our proposed enhanced integrated system, which is configuration 3 further enhanced by integrating BLESs, $O(4^2 + (4 + x)^{2.4})$, where x is the number of signals received from strong-signal BLE transmitters.

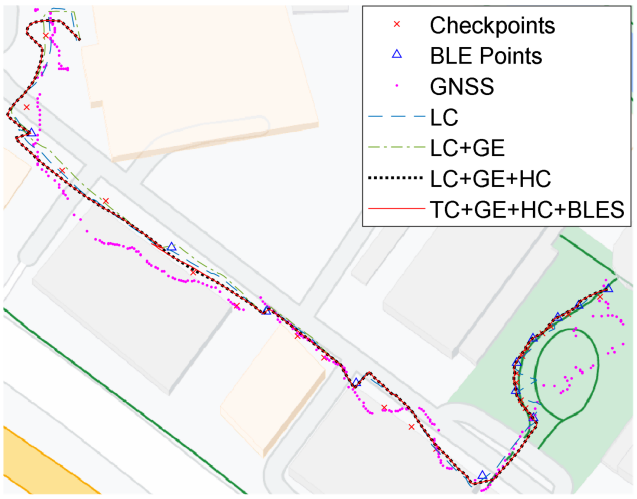

Fig. 11. Position performance comparison of different configurations in TC EKF on a smartphone without BLE RB (LC: loosely coupled, TC: tightly coupled, GE: GNSS errors estimation, HC: heading calculation, BLES: TC integration with BLESs).

The performances of these configurations over time can be seen in Fig. 11. The GNSS results, represented by pink dots, have noticeable deviations, particularly near buildings, and tend to be the most inaccurate, especially in areas with semi-outdoor conditions. The basic LC configuration, represented by the blue dashed line, offers more consistency than GNSS but still has occasional inaccuracies. The LC with GE estimation (LC + GE), depicted by a green dash-dotted line, improves upon the LC configuration, with a more consistent path and fewer deviations, especially around turns. The LC + GE integrated with HC (LC + GE + HC), marked by a black dotted line, ensures higher accuracy during straight-line movements when compared to LC + GE. The most accurate positioning is observed with the TC + GE + HC + BLES system, displayed by the red solid line, which maximizes the benefits of BLESs in its TC integration.

To quantitatively evaluate the positioning accuracy of the aforementioned configurations, (26) is used to compute the root mean square error (RMSE) with the location of checkpoints

$$\mathrm{RMSE} = \sqrt{\frac{1}{N}\sum_{i=1}^{N}\left[\left(\hat{x}_i - x_i\right)^2 + \left(\hat{y}_i - y_i\right)^2\right]} \tag{26}$$

where N is the number of points, i is the index of the points, $\hat{x}_i$, $\hat{y}_i$ are the calculated positions at checkpoints, and x_i, y_i are the measured positions at checkpoints.

The details are illustrated in Table III. The standalone GNSS exhibits significant errors in all directions, with RMSE values of 7.12, 16.85, and 18.29 m in the north, east, and horizontal directions, respectively. Due to PDR's ability to constrain GNSS's large fluctuations and BLE proximity's capability to correct significant GNSS deviations, the LC configuration demonstrates a considerable reduction in these errors, achieving RMSE values of 3.74 m in the north, 3.63 m in the east,

TABLE III
RMSE OF DIFFERENT SYSTEM CONFIGURATIONS IN TC EKF ON A SMARTPHONE WITHOUT BLE RB

Configuration	RMSE_N (m)	RMSE_E (m)	RMSE_T (m)	Max_T (m)	Median_T (m)
GNSS	7.12	16.85	18.29	35.65	14.47
LC	3.74	3.63	5.21	10.34	4.11
LC+GE	3.68	3.03	4.77	9.89	3.51
LC+GE+HC	2.87	3.30	4.37	9.78	3.29
TC+GE+HC+BLES	2.85	3.24	4.31	9.50	3.29

$RMSE_N$: RMSE in North, $RMSE_E$: RMSE in East, $RMSE_T$: Total RMSE in Horizontal, Max_T : Max Error in Horizontal, Median_T : Median Error in Horizontal, LC: Loosely Coupled, TC: Tightly Coupled, GE: GNSS Errors Estimation, HC: Heading Calculation, BLES: TC Integration with BLE Signals

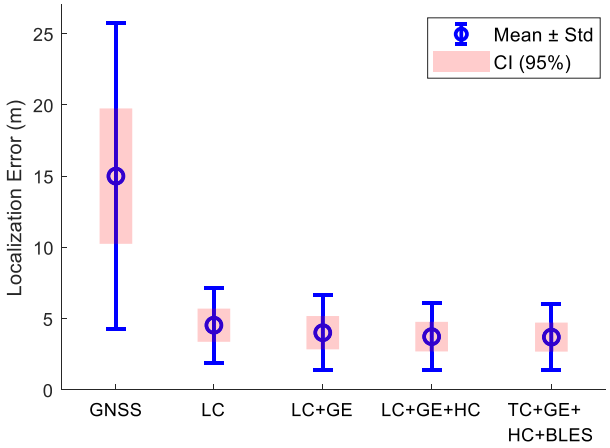

Fig. 12. Comparison of localization errors across different configurations in TC EKF on a smartphone without BLE RB (Std: standard deviation, CI: confidence interval, LC: loosely coupled, TC: tightly coupled, GE: GNSS errors estimation, HC: heading calculation, BLES: TC integration with BLESs).

and 5.21 m in total horizontal RMSE. When GE estimation is integrated into the LC configuration (LC + GE), the weight of GNSS in the EKF can be accurately set, reducing the impact of GEs on the overall results. Consequently, there is a further reduction in errors, particularly notable in the east direction, bringing them down to 3.68, 3.03, and 4.77 m for north, east, and total horizontal RMSE, respectively. The addition of HC (LC + GE + HC) refines the estimation of the pedestrian's walking direction, improving the horizontal RMSE to 4.37 m. With distances estimated from strong-signal BLE transmitters, the accumulated error in the forward direction of PDR can be further reduced. Hence, the TC + GE + HC + BLES configuration achieves optimal performance, with a total horizontal RMSE of 4.31 m. This level of accuracy meets the requirements for regional positioning, providing accurate navigation and positioning services for citizens moving between buildings in dense urban areas. It addresses the problem of pedestrians struggling to find their way due to a lack of precise location information in urban districts. In addition, it enables real-time supervision and management of personnel within such areas.

A detailed comparison of localization errors calculated from 22 checkpoints across various configurations is provided in Fig. 12. The circles represent the mean errors, and the blue error bars indicate the standard deviations. The pink-shaded areas correspond to the 95% confidence intervals

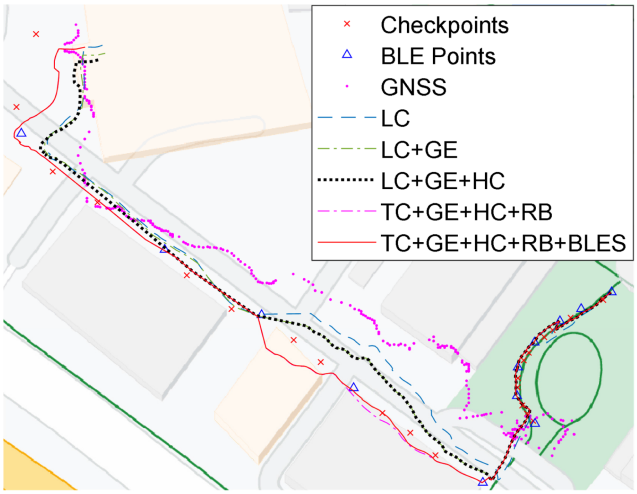

Fig. 13. Position performance comparison of different configurations in TC EKF on a smartphone with BLE RB (LC: loosely coupled, TC: tightly coupled, GE: GNSS errors estimation, HC: heading calculation, RB: BLE RSSI bias estimation, BLES: TC integration with BLESs).

(CIs) for each configuration, computed using the Student's t-distribution. It demonstrates that the GNSS configuration shows the highest mean error and variability. The introduction of LC, GE, and HC effectively reduces both the mean errors and their variability. Notably, the TC configuration, TC + GE + HC + BLES, achieves the smallest errors and variability.

C. Evaluation of Positioning Performance Enhancement of the Proposed Algorithms on a Smartphone With BLE RB

To evaluate the performance of our proposed algorithms, including the RB estimation algorithm, on a smartphone with inherent RB, we utilized the Huawei Mate 20 Pro for testing. This device, with its RB previously examined in Section IV-A, was used to traverse the same route detailed in Section IV-B. For a thorough comparison and assessment, five different GNSS/PDR/BLE integration configurations were selected. The computational complexity of these configurations is also listed in the form of $O(n^2 + k^{2.4})$, where n is the dimension of the state vector, and k is the dimension of the measurement vector.

1) *LC:* Basic LC GNSS/PDR/BLE integration from our prior study, $O(4^2 + 4^{2.4})$.
2) *LC + GE:* LC with GE estimation, $O(4^2 + 4^{2.4})$.
3) *LC + GE + HC:* LC with GE estimation and HC, $O(4^2 + 4^{2.4})$.
4) *TC + GE + HC + RB:* TC integration with GE estimation, HC, and BLE RB estimation, $O(5^2 + (4 + x)^{2.4})$, where x is the number of signals received from strong-signal BLE transmitters.
5) *TC + GE + HC + RB + BLES:* Our proposed enhanced integrated system, which is configuration 4 further enhanced by integrating BLESs, $O(5^2 + (4 + x)^{2.4})$, where x is the number of signals received from strong-signal BLE transmitters.

The effectiveness of these configurations through time is illustrated in Fig. 13. GNSS, shown with pink dots, displays significant variations, most notably around structures, and is generally the least precise, particularly in semi-outdoor environments. The basic LC configuration, indicated by the

TABLE IV
RMSE OF DIFFERENT SYSTEM CONFIGURATIONS IN TC EKF ON A SMARTPHONE WITH RB

Configuration	$RMSE_N$ (m)	$RMSE_E$ (m)	$RMSE_T$ (m)	Max_T (m)	$Median_T$ (m)
GNSS	22.99	16.17	28.10	52.71	25.32
LC	3.94	8.99	9.81	20.22	5.43
LC+GE	3.39	7.91	8.60	18.70	3.99
LC+GE+HC	3.86	7.44	8.38	18.04	3.99
TC+GE+HC+RB	4.03	2.90	4.96	9.90	3.99
TC+GE+HC+RB+BLES	3.79	2.79	4.71	9.89	3.29

$RMSE_N$: RMSE in North, $RMSE_E$: RMSE in East, $RMSE_T$: Total RMSE in Horizontal, Max_T : Max Error in Horizontal, $Median_T$: Median Error in Horizontal, LC: Loosely Coupled, TC: Tightly Coupled, GE: GNSS Errors Estimation, HC: Heading Calculation, RB: BLE RSSI Bias Estimation, BLES: TC Integration with BLE Signals

blue dashed line, shows a marked enhancement compared to GNSS. However, due to the nondetection of several weak-signal BLE transmitters, the cumulative error over time remains substantial. With the inclusion of GE estimation, the LC + GE system, visualized by the green dash-dotted line, further refines the position, sticking more closely to the checkpoints. The LC + GE + HC system, indicated by the black dotted line, benefits from added HC, refining the accuracy notably along straight paths. However, these enhancements only decelerate error accumulation without effectively rectifying it. The TC + GE + HC + RB system, shown as the purple dash-dotted line, demonstrates even better accuracy, attributable to detecting more weak-signal BLE transmitters since the BLE RB is considered. Most impressively, the TC + GE + HC + RB + BLES system, displayed by the red solid line, achieves the best accuracy, maximizing the benefits of BLESs in its TC integration.

By using (26), the quantitatively evaluate the positioning accuracy can be obtained. The details are illustrated in Table IV. The GNSS system exhibits the highest RMSE values across all directions, with 22.99, 16.17, and 28.10 m for north, east, and horizontal, respectively. This clearly indicates its limited accuracy in complex environments. Upon integrating GNSS with PDR and BLE using the LC method, a significant enhancement is observed, reducing the RMSE to 3.94, 8.99, and 9.81 m in the respective directions. Further assisting this configuration with GE estimation (LC + GE) brings about further improvements, especially in the east direction, with the RMSE declining to 7.91 m. The addition of HC (LC + GE + HC) slightly increases the RMSE in the north to 3.86 m but refines the east and horizontal values to 7.44 and 8.38 m, respectively.

Upon utilizing the TC approach to estimate the BLE RB and incorporating it into the system (TC + GE + HC + RB), a heightened detection of weak-signal BLE transmitters is observed. This translates to more frequent position corrections, leading to a significant improvement in accuracy. As a result, the horizontal RMSE is sharply reduced to 4.96 m. However, due to the combined effects of heading errors and proximity detection method errors, some directional errors may increase. For instance, the RMSE in the north rises to 4.03 m. Furthermore, the inclusion of BLESs in the integration (TC + GE + HC + RB + BLES) produces the most precise

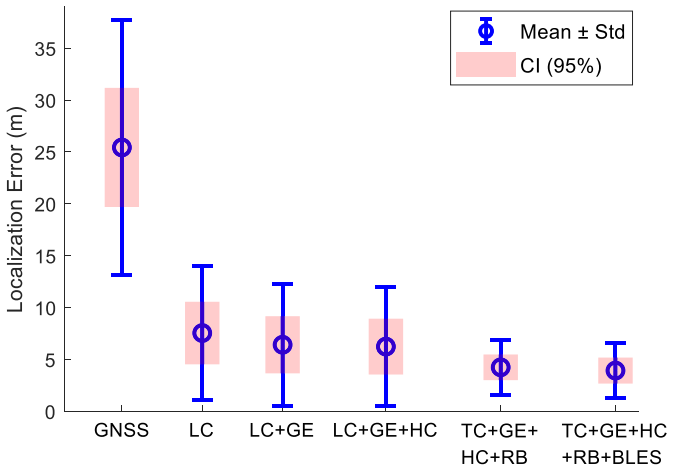

Fig. 14. Comparison of localization errors across different configurations in TC EKF on a smartphone with BLE RB (Std: standard deviation, CI: confidence interval, LC: loosely coupled, TC: tightly coupled, GE: GNSS errors estimation, HC: heading calculation, RB: BLE RSSI bias estimation, BLES: TC integration with BLESs).

results across the configurations with RMSE values of 3.79, 2.79, and 4.71 m for north, east, and horizontal directions, respectively. This demonstrates that when using a smartphone exhibiting RB, our algorithm can still achieve the same level of performance as when using a smartphone without RB.

The localization errors calculated from 22 checkpoints for various configurations are compared in detail, as shown in Fig. 14. The circles indicate the mean errors, while the blue error bars represent the standard deviations. The pink-shaded regions depict the 95% CIs, calculated using the Student's t-distribution. The results demonstrate that the GNSS configuration has the greatest mean error and variability. Although LC with GE and HC configurations help reduce both the mean errors and their variability to some extent, the final errors remain relatively large due to the presence of BLE RB. The TC configurations, which include RB estimation for the smartphone's BLE sensor, effectively address this issue. The TC + GE + HC + RB + BLES configuration, which integrates distances estimated from strong-signal BLE transmitters, achieves the smallest errors and variability, matching the performance observed when using a smartphone without RB. This result demonstrates the effectiveness of the proposed algorithm.

V. CONCLUSION

In this article, we have proposed a TC BLE-enhanced GNSS/PDR system designed to provide accurate pedestrian location services in urban and semi-outdoor environments. The system involves monitoring GNSS quality through the utilization of BLESs and PDR results, followed by the integration of the smartphone's orientation with BLE-derived heading estimates to determine the pedestrian's walking direction. The final step encompasses the estimation of the RB of the BLE sensor and the reduction of cumulative PDR positioning errors using a TC Kalman filter that incorporates distance measurements from strong-signal BLE transmitters.

Our extensive experiments conducted in Hong Kong have demonstrated the effectiveness and robustness of our proposed system.

1) The adaptive and accurate evaluation of GNSS quality through the combined use of BLE and PDR mitigates the adverse impact of erroneous GNSS positioning results on the fused positioning outcomes.
2) The amalgamation of the smartphone's orientation with BLE-derived headings provides an accurate estimation of the pedestrian's walking direction for PDR computations, significantly boosting positioning accuracy, particularly in linear trajectories.
3) The TC approach enhances the estimation of RB of the smartphone's BLE sensor, leading to a marked improvement in the detection of weak-signal BLE transmitters and resulting in a substantial 41% reduction in horizontal positioning errors.
4) The integration of distance measurements from strong-signal BLE transmitters in the TC framework as supplementary observations improves positioning accuracy, even with fewer than four BLESs available.

In conclusion, our enhanced TC GNSS/PDR/BLE integration system offers a robust solution for precise pedestrian positioning in challenging environments, unaffected by device heterogeneity. Future research will focus on applying this algorithm to achieve seamless indoor-outdoor positioning transitions and establishing pedestrian networks to provide road information to our integrated system, further enhancing pedestrian positioning performance.

REFERENCES

[1] F. Rahman, E. Aghapour, and J. A. Farrell, "Vehicle ECEF position accuracy and reliability in the presence of DGNSS communication latency," *IEEE Intell. Transp. Syst. Mag.*, vol. 13, no. 4, pp. 262–272, Winter. 2021.

[2] D. Weng, W. Chen, Y. Lu, S. Ji, H. Luo, and M. Cai, "Global DGNSS service for mobile positioning through public corrections," *Adv. Space Res.*, vol. 72, no. 10, pp. 4402–4412, 2023.

[3] L. T. Hsu, "Analysis and modeling GPS NLOS effect in highly urbanized area," *GPS Solutions*, vol. 22, no. 1, p. 7, Nov. 2017.

[4] P. D. Groves and Z. Jiang, "Height aiding, C/N0 weighting and consistency checking for GNSS NLOS and multipath mitigation in urban areas," *J. Navig.*, vol. 66, no. 5, pp. 653–669, Sep. 2013.

[5] C. Jiang et al., "Implementation and performance analysis of the PDR/GNSS integration on a smartphone," *GPS Solutions*, vol. 26, no. 3, p. 81, Jul. 2022.

[6] M. Chowdhary, M. Sharma, A. Kumar, S. Dayal, and M. Jain, "Method and apparatus for determining walking direction for a pedestrian dead reckoning process," U.S. Patent 10 302 434, May 28, 2019.

[7] Q. Zeng, J. Wang, Q. Meng, X. Zhang, and S. Zeng, "Seamless pedestrian navigation methodology optimized for indoor/outdoor detection," *IEEE Sensors J.*, vol. 18, no. 1, pp. 363–374, Jan. 2018.

[8] A. Mansour et al., "Everywhere: A framework for ubiquitous indoor localization," *IEEE Internet Things J.*, vol. 10, no. 6, pp. 5095–5113, Mar. 2023.

[9] Y. Zhang, X. Tan, and C. Zhao, "UWB/INS integrated pedestrian positioning for robust indoor environments," *IEEE Sensors J.*, vol. 20, no. 23, pp. 14401–14409, Dec. 2020, doi: 10.1109/JSEN.2020.2998815.

[10] F. Subhan et al., "Experimental analysis of received signals strength in Bluetooth low energy (BLE) and its effect on distance and position estimation," *Trans. Emerg. Telecommun. Technol.*, vol. 33, no. 2, p. e3793, 2022.

[11] J. Ye, Y. Li, H. Luo, J. Wang, W. Chen, and Q. Zhang, "Hybrid urban canyon pedestrian navigation scheme combined PDR, GNSS and beacon based on smartphone," *Remote Sens.*, vol. 11, no. 18, p. 2174, Sep. 2019.

[12] H. Luo et al., "Integration of GNSS and BLE technology with inertial sensors for real-time positioning in urban environments," *IEEE Access*, vol. 9, pp. 15744–15763, 2021.

[13] L. Icking, T. Kersten, and S. Schön, "Evaluating the urban trench model for improved GNSS positioning in urban areas," in *Proc. IEEE/ION Position, Location Navig. Symp. (PLANS)*, Apr. 2020, pp. 631–638.

[14] Z. Dai and F. J. W. Podd, "A power-efficient BLE augmented GNSS approach to site-specific navigation," in *Proc. IEEE/ION Position, Location Navig. Symp. (PLANS)*, Apr. 2020, pp. 1305–1310.

[15] T.-M.-T. Dinh, N.-S. Duong, and Q.-T. Nguyen, "Developing a novel real-time indoor positioning system based on BLE beacons and smartphone sensors," *IEEE Sensors J.*, vol. 21, no. 20, pp. 23055–23068, Oct. 2021.

[16] Y. You and C. Wu, "Hybrid indoor positioning system for pedestrians with swinging arms based on smartphone IMU and RSSI of BLE," *IEEE Trans. Instrum. Meas.*, vol. 70, pp. 1–15, 2021.

[17] P. Pascacio, J. Torres–Sospedra, S. Casteleyn, and E. S. Lohan, "A collaborative approach using neural networks for BLE-RSS lateration-based indoor positioning," in *Proc. Int. Joint Conf. Neural Netw. (IJCNN)*, Jul. 2022, pp. 1–9.

[18] X.-Y. Lin, T.-W. Ho, C.-C. Fang, Z.-S. Yen, B.-J. Yang, and F. Lai, "A mobile indoor positioning system based on iBeacon technology," in *Proc. 37th Annu. Int. Conf. IEEE Eng. Med. Biol. Soc. (EMBC)*, Aug. 2015, pp. 4970–4973.

[19] F. Yin, Y. Zhao, and F. Gunnarsson, "Proximity report triggering threshold optimization for network-based indoor positioning," in *Proc. 18th Int. Conf. Inf. Fusion (Fusion)*, Washington, DC, USA, Jul. 2015, pp. 1061–1069.

[20] S. S. Chawathe, "Low-latency indoor localization using Bluetooth beacons," in *Proc. 12th Int. IEEE Conf. Intell. Transp. Syst.*, Oct. 2009, pp. 1–7.

[21] W. Navidi, W. S. Murphy Jr., and W. Hereman, "Statistical methods in surveying by trilateration," *Comput. Statist. Data Anal.*, vol. 27, no. 2, pp. 209–227, 1998, doi: 10.1016/S0167-9473(97)00053-4.

[22] D. Giovanelli, E. Farella, D. Fontanelli, and D. Macii, "Bluetooth-based indoor positioning through ToF and RSSI data fusion," in *Proc. Int. Conf. Indoor Positioning Indoor Navig. (IPIN)*, Nantes, France, Sep. 2018, pp. 1–8.

[23] T.-M. T. Dinh, N.-S. Duong, and K. Sandrasegaran, "Smartphone-based indoor positioning using BLE iBeacon and reliable lightweight fingerprint map," *IEEE Sensors J.*, vol. 20, no. 17, pp. 10283–10294, Sep. 2020, doi: 10.1109/JSEN.2020.2989411.

[24] A. K. M. M. Hossain, Y. Jin, W.-S. Soh, and H. N. Van, "SSD: A robust RF location fingerprint addressing mobile Devices' heterogeneity," *IEEE Trans. Mobile Comput.*, vol. 12, no. 1, pp. 65–77, Jan. 2013.

[25] D. H. Titterton and J. L. Weston, *Strapdown Inertial Navigation Technology*, 2nd ed. Herts, U.K.: Institute of Electrical Engineering, 2004.

[26] X. L. Tao, F. Zhu, X. Hu, W. K. Liu, and X. H. Zhang, "An enhanced foot-mounted PDR method with adaptive ZUPT and multi-sensors fusion for seamless pedestrian navigation," *GPS Solutions*, vol. 26, no. 1, p. 13, Jan. 2022.

[27] D. Yan, C. Shi, T. Li, and Y. Li, "FlexPDR: Fully flexible pedestrian dead reckoning using online multimode recognition and time-series decomposition," *IEEE Internet Things J.*, vol. 9, no. 16, pp. 15240–15254, Aug. 2022.

[28] L. Fang et al., "Design of a wireless assisted pedestrian dead reckoning system–the NavMote experience," *IEEE Trans. Instrum. Meas.*, vol. 54, no. 6, pp. 2342–2358, Dec. 2005, doi: 10.1109/TIM.2005.858557.

[29] P. Goyal, V. J. Ribeiro, H. Saran, and A. Kumar, "Strap-down pedestrian dead-reckoning system," in *Proc. Int. Conf. Indoor Positioning Indoor Navig.*, Guimarães, Portugal, Sep. 2011, pp. 1–7.

[30] X. Kang, B. Huang, and G. Qi, "A novel walking detection and step counting algorithm using unconstrained smartphones," *Sensors*, vol. 18, no. 1, p. 297, Jan. 2018.

[31] J.-H. Wang, J.-J. Ding, Y. Chen, and H.-H. Chen, "Real time accelerometer-based gait recognition using adaptive windowed wavelet transforms," in *Proc. IEEE Asia–Pacific Conf. Circuits Syst.*, Dec. 2012, pp. 591–594.

[32] L. E. Díez, A. Bahillo, J. Otegui, and T. Otim, "Step length estimation methods based on inertial sensors: A review," *IEEE Sensors J.*, vol. 18, no. 17, pp. 6908–6926, Sep. 2018, doi: 10.1109/JSEN.2018.2857502.

[33] S. Godha, G. Lachapelle, and M. E. Cannon, "Integrated GPS/INS system for pedestrian navigation in a signal degraded environment," in *Proc. I_{ON} GNSS*, Fort Worth, TX, USA, Sep. 2006, pp. 26–29.

[34] R. Chen, L. Pei, and Y. Chen, "A smart phone based PDR solution for indoor navigation," in *Proc. 24th Int. Tech. Meeting Satell. Division Inst. Navig. (ION GNSS+)*, Portland, OR, USA, Sep. 2011, pp. 1404–1408.

[35] H. Weinberg, "Using the ADXL202 in pedometer and personal navigation applications," *Analog Devices AN-602 Appl. Note*, vol. 2, no. 2, pp. 1–6, 2002.
[36] W. Chen, R. Chen, Y. Chen, H. Kuusniemi, and J. Wang, "An effective pedestrian dead reckoning algorithm using a unified heading error model," in *Proc. IEEE/ION Position, Location Navig. Symp.*, Indian Wells, CA, USA, May 2010, pp. 340–347.
[37] J.-S. Hu and K.-C. Sun, "A robust orientation estimation algorithm using MARG sensors," *IEEE Trans. Instrum. Meas.*, vol. 64, no. 3, pp. 815–822, Mar. 2015, doi: 10.1109/TIM.2014.2359815.
[38] U. Steinhoff and B. Schiele, "Dead reckoning from the pocket—An experimental study," in *Proc. IEEE Int. Conf. Pervasive Comput. Commun. (PerCom)*, Mannheim, Germany, Mar. 2010, pp. 162–170.
[39] M. Kourogi and T. Kurata, "A method of pedestrian dead reckoning for smartphones using frequency domain analysis on patterns of acceleration and angular velocity," in *Proc. IEEE/ION Position, Location Navig. Symp. (PLANS)*, Monterey, CA, USA, May 2014, pp. 164–168.
[40] C. Combettes and V. Renaudin, "Walking direction estimation based on statistical modeling of human gait features with handheld MIMU," *IEEE/ASME Trans. Mechatronics*, vol. 22, no. 6, pp. 2502–2511, Dec. 2017.
[41] Q. Tian, K. I. Wang, and Z. Salcic, "A resetting approach for INS and UWB sensor fusion using particle filter for pedestrian tracking," *IEEE Trans. Instrum. Meas.*, vol. 69, no. 8, pp. 5914–5921, Aug. 2020.
[42] M. St-Pierre and D. Gingras, "Comparison between the unscented Kalman filter and the extended Kalman filter for the position estimation module of an integrated navigation information system," in *Proc. IEEE Intell. Vehicles Symp.*, Jun. 2004, pp. 831–835.
[43] X. Kong, C. Wu, Y. You, and Y. Yuan, "Hybrid indoor positioning method of BLE and PDR based on adaptive feedback EKF with low BLE deployment density," *IEEE Trans. Instrum. Meas.*, vol. 72, pp. 1–12, 2023.
[44] W. Qiu, Q. Zeng, R. Xu, J. Liu, J. Shi, and Q. Meng, "A multipath mitigation algorithm for GNSS signals based on the steepest descent approach," *Satell. Navig.*, vol. 3, no. 1, p. 14, Jul. 2022.
[45] A. Rehman, H. Shahid, M. A. Afzal, and H. M. A. Bhatti, "Accurate and direct GNSS/PDR integration using extended Kalman filter for pedestrian smartphone navigation," *Gyroscopy Navig.*, vol. 11, no. 2, pp. 124–137, Apr. 2020.
[46] Y. Yu et al., "A bi-LSTM approach for modelling movement uncertainty of crowdsourced human trajectories under complex urban environments," *Int. J. Appl. Earth Observ. Geoinf.*, vol. 122, Aug. 2023, Art. no. 103412.
[47] X. Wang et al., "Tightly coupled integration of pedestrian dead reckoning and Bluetooth based on filter and optimizer," *IEEE Internet Things J.*, vol. 10, no. 8, pp. 7327–7342, Apr. 2023.
[48] April Brother Technology Co. *CE, FCC Available Road Stud Beacon*. [Online]. Available: https://store.aprbrother.com/product/road-stud-beacon

Jingxian Wang received the B.S. and M.S. degrees from Nanjing University of Aeronautics and Astronautics, Nanjing, China, in 2015 and 2018, respectively, and the Ph.D. degree from The Hong Kong Polytechnic University, Hong Kong, in 2023.

He is currently a Post-Doctoral Fellow with the Department of Land Surveying and Geo-Informatics, The Hong Kong Polytechnic University. His research interests include multisensor fusion, indoor positioning, pedestrian navigation, and vehicle navigation.

Xiaolong Mi received the Ph.D. degrees from the University of Chinese Academy of Sciences, Beijing, China, in 2022, and Curtin University, Perth, Australia, in 2023.

He is currently a Research Assistant Professor with the Department of Land Surveying and Geo-Informatics, The Hong Kong Polytechnic University, Hong Kong. His research interests include global navigation satellite system (GNSS) and low Earth orbit (LEO) technologies for positioning, navigation, and timing (PNT) along with the application of artificial intelligence (AI) in Earth and space sciences.

Wu Chen received the Ph.D. degree from Newcastle University, Newcastle upon Tyne, U.K., in 1992.

He is currently a Professor with the Department of Land Surveying and Geo-Informatics, The Hong Kong Polytechnic University, Hong Kong. His current research interests include the global navigation satellite system (GNSS) positioning quality evaluation, system integrity, various GNSS applications, seamless positioning, and simultaneous localization and mapping (SLAM).

Huan Luo received the B.S. and M.S. degrees in geomatics engineering from Northeastern University, Shenyang, China, in 2013 and 2015, respectively, and the Ph.D. degree from the Department of Land Surveying and Geo-Informatics (LSGI), The Hong Kong Polytechnic University (PolyU), Hong Kong, in 2020.

She is currently a Post-Doctoral Fellow with PolyU. Her research interests include global navigation satellite system (GNSS) positioning in challenging environments, multipath mitigation, and multisensor integration for pedestrian localization.

Ahmed Mansour received the B.Sc. and M.Sc. degrees in civil engineering and geomatics from Cairo University, Cairo, Egypt, in 2013 and 2017, respectively, and the Ph.D. degree from The Hong Kong Polytechnic University (PolyU), Hong Kong, in 2023.

He is currently a Post-Doctoral Fellow with the Department of Land Surveying and Geo-Informatics (LSGI), PolyU. His research interests include indoor positioning, multisensor fusion, crowdsourcing, and cooperative positioning.

Dr. Mansour has received the Hong Kong Ph.D. Fellowship in 2017.

Yaxin Li received the B.S. degree from Wuhan University, Wuhan, China, in 2013, and the M.S. and Ph.D. degrees from The Hong Kong Polytechnic University, Hong Kong, in 2015 and 2020, respectively.

His current research interests include indoor positioning and navigation, simultaneous localization and mapping (SLAM), indoor 3-D modeling, semantic segmentation, and auto building information modeling (BIM) generation.

Yue Yu received the Ph.D. degrees from Wuhan University, Wuhan, China, in 2021, and The Hong Kong Polytechnic University, Hong Kong, in 2022.

He is currently a Research Assistant Professor with the Department of Land Surveying and Geo-Informatics, The Hong Kong Polytechnic University. He has published more than 50 journal articles and conference papers and has applied for more than 20 patents and software copyrights. His research interests include urban informatics, seamless positioning and navigation, mobile mapping, and geo-spatial data analytics.

Duojie Weng (Member, IEEE) received the B.S. and M.S. degrees in electrical engineering from Hohai University, Nanjing, China, in 2007 and 2010, respectively, and the Ph.D. degree from The Hong Kong Polytechnic University, Hong Kong, in 2016.

He is currently a Research Assistant Professor with the Department of Land Surveying and Geo-Informatics, The Hong Kong Polytechnic University. His research interests include integrity monitoring of global navigation satellite system (GNSS), kinematic global positioning system (GPS), sensor integration for various navigation systems, and urban positioning.